eTransportation 6 (2020) 100087

Contents lists available at ScienceDirect

eTransportation

journal homepage: www.journals.elsevier.com/etransportation

Safety assessment of electrically cycled cells at high temperatures under mechanical crush loads

Georgi Kovachev [a, *], Christian Ellersdorfer [a], Gregor Gstrein [a], Ilie Hanzu [b, c], H. Martin R. Wilkening [b, c], Tobias Werling [d], Florian Schauwecker [d], Wolfgang Sinz [a]

[a] Vehicle Safety Institute, Graz University of Technology, Inffeldgasse 23/I, A-8010, Graz, Austria
[b] Institute for Chemistry and Technology of Materials, Graz University of Technology, Stremayrgasse 9, A-8010, Graz, Austria
[c] Alistore – European Research Institute, CNRS FR3104, Hub de l'Energie, Rue baudelocque, 80039, Amiens, France
[d] Mercedes-Benz AG, Mercedesstraße 120, D-70372, Stuttgart, Germany

ARTICLE INFO

Article history:
Received 2 July 2020
Received in revised form
25 September 2020
Accepted 18 October 2020
Available online 26 October 2020

Keywords:
Lithium ion battery
Cycle ageing
Degradation mechanisms
Mechanical properties change
Quasi-static indentation load
Crash safety

ABSTRACT

An ageing test procedure was developed in this work in order to assess the influence of battery degradation effects, occurring during electrical cycling of lithium-ion batteries at elevated temperatures, on the electrical and mechanical properties of the cells and on their safety behaviour under mechanical quasi-static crush loading. Commercial 41 A h NMC-LMO/graphite pouch cells were charged and discharged at 60 °C for 700 cycles at 1 C in an SOC range between 10 and 90%. Electrical properties of these batteries were evaluated every 100 cycles at room temperature. By the end of the cycling procedure, a 27% reduction of the initial capacity was observed. The behaviour of the fully charged aged cells under a quasi-static mechanical load was examined in a series of indentation tests, using a flat impactor geometry. This behaviour was compared to that of fresh cells. Test results show that all investigated electrically cycled cells exhibited a slight decrease in stiffness. Aged batteries also failed at higher compressive strengths and larger deformations. Post-mortem analysis of the aged cells was performed as a next step using scanning electron microscopy and the occurred degradation effects were evaluated in order to explain the changes observed in the battery electrical and mechanical properties.
© 2020 The Author(s). Published by Elsevier B.V. This is an open access article under the CC BY license (http://creativecommons.org/licenses/by/4.0/).

1. Introduction

Lithium ion batteries (LIB) are typically characterised by their high energy density and long battery life, which makes them the most promising energy storage system for electric vehicles (EV) currently available [1]. However, as they undergo an increasing number of charging/discharging cycles, the batteries in EV degrade [2], resulting in changes in battery performance and electrical characteristics. During their cycle lifetime, the useable capacity of LIB decreases, causing a reduction in the achievable mileage with a single charge. The rate at which lithium ion batteries degrade is not only closely associated with the cell chemistry and design, but also to the operating conditions to which it is subjected. In general, most lithium ion battery chemistries have an ideal working temperature range of 15–35 °C [3]. The battery management system (BMS) regulates the temperature of each cell to stay in this range in order to prevent the battery from overheating or freezing. If higher temperatures are reached, however, this will accelerate battery degradation and lead to higher capacity losses [4,5] due to the increased rate of solid electrolyte interphase (SEI) formation and faster consumption of the liquid electrolyte in chemical side reactions [6]. High temperature cycling also provokes higher amounts of mechanical stress in the particles of the active material of the cathode and can lead to particle cracking, oxygen release and loss of lithium [7].

Stiaszny et al. [8]. Conducted a capacity fade analysis on commercial lithium ion batteries with a mixed $LiMnO_4$/NMC cathode. The loss of mobile lithium due to SEI layer formation on the anode was identified as the most significant degradation mechanism, which was responsible for the high capacity losses and an increase in the internal resistance (IR) of the cells. Ren et al. [9]. Presented very similar results for lithium ion pouch batteries with analogous

* Corresponding author.
E-mail addresses: georgi.kovachev@tugraz.at (G. Kovachev), christian.ellersdorfer@tugraz.at (C. Ellersdorfer), gregor.gstrein@tugraz.at (G. Gstrein), hanzu@tugraz.at (I. Hanzu), wilkening@tugraz.at (H.M.R. Wilkening), wolfgang.sinz@tugraz.at (W. Sinz).

https://doi.org/10.1016/j.etran.2020.100087
2590-1168/© 2020 The Author(s). Published by Elsevier B.V. This is an open access article under the CC BY license (http://creativecommons.org/licenses/by/4.0/).

chemistry. In their study, they showed that the loss of lithium inventory (LLI), which is caused by the growth of the SEI film, and the loss of active material (LAM) are the main factors that lead to battery performance degradation. The loss of active material was found to correlate with the electrolyte and binder decomposition inside the cells as well as with the loss of contact between active materials and electrodes due to current collector corrosion.

The above-mentioned degradation mechanisms reduce the useable electrical capacity of lithium-ion batteries; however, it is not known in detail how these mechanisms affect the mechanical response of the cells and their safety behaviour under mechanical loads. In the literature, cycle ageing has been shown to have a negative effect on the mechanical properties of individual electrodes in specific load cases [10]. A reduction in the compressive and tensile stress at failure for battery anodes was observed by Wu et al. [10], as well as a decrease in the Young's modulus in the initial stage of the mechanical compression tests conducted on aged positive and negative electrodes. However, the authors did not perform a detailed analysis of the degradation mechanisms leading to a changed behaviour, and no information was given regarding how component degradation influences the mechanical and safety behaviour of a single cell. Cycle-aged elliptical metal-can batteries, studied by Zhang et al. [11], showed a reduction in the maximum force at failure under a mechanical load. The intercalation of particles in the separator pores was identified as the main reason for the loss of the puncture strength of the insulating separator layer and for the accelerated cell failure. However, the degradation process was not investigated in detail for every battery component, and no safety assessment was provided.

The goal of conducting this research was to evaluate the influence of specific degradation mechanisms that occur during high-temperature battery cycling on the mechanical response of lithium ion pouch cells when the latter are subjected to quasi-static crush loads. This allowed us to provide an accurate safety assessment of aged batteries. Ageing effects on each of the individual battery components were visualised and analysed by the means of scanning electron microscopy (SEM). The results are not only used to explain changes in the measured indentation force/displacement curves, but also to evaluate the effect of battery degradation mechanisms on thickness changes in individual electrodes and throughout the whole battery. The safety assessment of electrically aged cells is made based on the evaluation of the severity of the thermal runaway process and the mechanical response of the batteries during quasi-static indentation tests.

2. Method

In this section, a short description is provided for the electrical ageing procedure of the investigated batteries and the methodology used for their electrical characterisation. A method to measure the increase in the thickness of the cells before and after ageing is also presented, as well as a description of the mechanical test bench that was used to conduct quasi-static indentation tests. At the end of this section, the method and test equipment used for the post-mortem analysis are briefly explained.

2.1. Electric ageing procedure

Commercially available lithium ion pouch cells were used in this study with a nominal capacity of 41 A h and a graphite/NMC-LMO electrode chemistry. A more detailed description of the battery structure and electrode size is provided in Ref. [12]. Each battery was positioned between two 10-mm-thick aluminium plates, in order to apply an evenly distributed pretension force on the electrode stack during the cycling procedure. This force was comparable to the one present in the battery module and was achieved by tightening six screws per cell with a torque of 1 Nm, resulting in the application of 3 kN (0.06 N/mm^2 surface pressure) distributed across on the whole electrode stack. To stabilize the cells before starting the cycling procedure, all cells were charged and discharged ten times between 4.2 V and 2.5 V at room temperature (25 °C) with a C-rate of 0.33C.

A Bitrode battery cycle life tester was used in this study to cycle all batteries at a temperature of 60 °C from 10 to 90% state of charge (SOC). These SOC values were chosen in order to avoid inducing additional ageing effects, which occur when the cell reaches the upper or lower voltage limits [6]. A constant current constant voltage (CCCV) charging protocol was used for charging of the batteries at a charging rate of 1C in the constant current phase and a cut-off current of 0.05 C in the constant voltage phase. Discharging was done in constant current (CC) mode with a discharge rate of 1C. Every 100 cycles, as well as at the beginning and at the end of the cycling procedure, all cells were characterised electrically at room temperature. The end criterion of the ageing program was set at 700 cycles.

2.2. Electrical reference performance tests

The electrical performance of the analysed batteries was characterised by conducting reference performance tests (RPT), which included measurements of the open circuit voltage (OCV) curve, the discharge capacity and investigation of the internal resistance and impedance of the system using electrochemical impedance spectroscopy (EIS) at a 50% state of charge.

At the start and end of the ageing program, the OCV curve of all batteries was measured for both charging and discharging. After an initial capacity check was performed, the cells were fully charged to their upper potential. The batteries were then discharged in SOC steps of 10% with reference to their nominal capacity, followed by an intermediate break of 3 h. After the break, the cells were assumed to be in a steady state, at which time the open-circuit voltage was measured. The discharging current rate between each step was set to 0.33C. In the range of 0−10% SOC, the step size was reduced to 2%. To determine the OCV of the batteries during the charging process, the inverse procedure of the one described above was used. Starting from a fully discharged state, batteries were charged stepwise up to 100% SOC, and the open circuit voltage was measured at each charging step after a 3-h rest.

Every 100 cycles, the discharge curve of the battery, its internal resistance and its impedance were evaluated. Discharge curve measurements were done at a discharging rate of 0.33C at room temperature in order to track any capacity changes that occurred due to electrochemical cycling. The evaluation of the internal resistance was conducted at 50% SOC. After reaching the desired charging condition, a discharge pulse of 3C was applied to the battery for 30 s. The internal resistance (R_i) of the battery was calculated by subtracting the voltage of the battery under load (U_l) from the voltage of the battery before applying the current pulse (U_0) and dividing this result by the discharge current value (I).

$$R_i = (U_0 - U_l)/I \quad (1)$$

Changes to the battery complex impedance were evaluated using electrochemical impedance spectroscopy. EIS measurements were conducted on a Digatron EIS meter in the frequency range of 10 mHz to 1 kHz after setting the battery SOC to 50%. All electrical reference tests were performed at a temperature of 25 °C.

2.3. Mechanical testing

Quasi-static mechanical abuse tests were conducted on fresh and aged cells with a specific hydraulic press with a displacement tolerance of ±1 μm. Tested cells were charged to 100% SOC and placed on top of a 1-mm-thick isolating Pertinax® plate (Kaindl, HP2061) in the chamber of the hydraulic press. A flat impactor with an initial indentation surface area of 10 mm × 234 mm was positioned in the middle of the battery and oriented in its longitudinal direction (u-direction in Fig. 1).

A small radius of 5 mm was introduced along the impactor edge to prevent the impactor shape from additionally influencing the test results. Such unconventional indenter form was selected because of the assumption that the surface of each layer inside the battery degrades heterogeneously. By enlarging the initial contact area the probability of testing in highly degraded area of the battery increases and thus also the chance of detecting changes in the behaviour of the battery under mechanical abuse conditions. Tests were conducted at a testing velocity of 1 mm/min under ambient temperature conditions, whereby every cell was deformed up to a maximum of 50% of the initial cell thickness. The mechanical resistance, displacement and cell voltage were recorded during all abuse tests at an acquisition frequency of 1 kHz. For this specific load case, a load cell type GMT Serie K 500 kN was used (accuracy class 0.02%) to measure the indentation force acting on the battery. Data acquisition was conducted using a NI-9237 Bridge Input Module with a resolution of 24 bits and a sample rate of 50 kS/s. To record voltage data of the battery, a 24-bit NI-9229 Voltage Input Module (0–60 V per channel) was used.

2.4. Thickness measurements of the cell

To evaluate battery thickness before and after the electrochemical cycling procedure, a portable 3D measurement device (FaroArm Platinum) was used. The device was first calibrated and then characterised by measuring a metal sheet with a thickness of 5 mm. The measurement accuracy was determined to be in the order of 50 μm. Cells were positioned flat on a measurement bench, and the thickness of each cell was determined at several different locations, as seen in Fig. 1. The mean cell thickness value, derived from all measurement points shown on the right-hand side in Fig. 1, was used for evaluation of battery thickness changes between fresh and aged batteries.

2.5. Post-mortem analysis

Post-mortem analysis was conducted on single battery components to identify any structural and dimensional changes in the internal battery layers. After the cells were disassembled and a detailed visual inspection was performed, small samples were generated from the battery anode, cathode and separator and investigated using scanning electron microscopy (SEM). High-resolution surface characterisation of the morphology was conducted using a ZEISS Ultra 55 Field Scanning Electron Microscope (FESEM). Energy Dispersive X-ray Spectroscopy (EDXS) spectra were acquired to determine the material composition using an EDAX Super Octane Silicon Drift Detection System. Broad Ion Beam (BIB) cutting was performed to prepare cross-sectional samples of the anode and the cathode, as well as to assess any thickness changes [12] in the layers due to battery degradation. The cross-section of the separator was prepared with the cryo-breaking technique. Briefly, the polypropylene membrane was deep-frozen with liquid nitrogen [13], and then the investigated layer was broken in a controlled manner. Samples in cross section were visualised by using the same imaging system as was used for the surface morphology investigations. Raman spectroscopy was conducted on aged copper (Cu) to obtain additional information about the chemical composition of the electrode surface and to identify any signs of corrosion on the current collector.

3. Results and discussion

In this section, the changes that occurred in the electrical and mechanical characteristics of the tested batteries due to cycle ageing are described in detail. The degradation mechanisms which occurred during cycling are visualised in a series of post-mortem analyses, and their influence on the battery behaviour is described. Also, correlations between the battery thickness increase and battery degradation are identified, and possible reasons for these correlations are pointed out and discussed.

3.1. Electrical changes

In Fig. 2, a comparison of the electrochemical cycling data between fresh and aged cells is visualised. After the ageing program was completed, an average capacity loss of about 27% was measured in all cells. This loss can be attributed to the constant loss of lithium inventory [6,14] and the loss of active material at the cathode [9]. During the cycling procedure, active lithium is consumed in chemical side reactions with the electrolyte, leading to the formation of a thicker SEI on the anode surface (Section 1.1.1.1). Due to the high temperature, these reactions occur at an increased rate, explaining the observed relatively high capacity loss of ~4% per 100 cycles (Fig. 2a). In addition, this particular cathode material, containing LMO ($LiMn_2O_4$), is known to age faster than pure NMC formulations. In Fig. 2b, a comparison is displayed between the discharge curves of fresh and aged cells. Because of the high amount of lithium lost, the curves shift to the left, which is a sign of reduced output energy the cells can deliver. Battery capacity loss was identified as about 27% after 700 cycles.

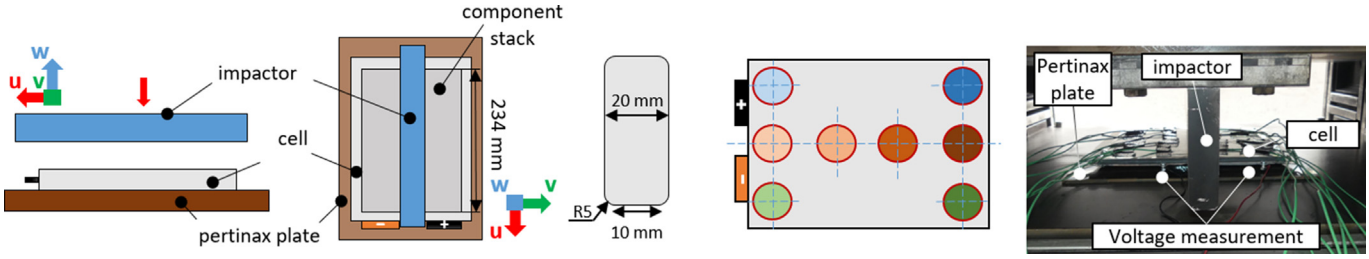

Fig. 1. Mechanical test setup used to evaluate battery safety before and after electrical ageing and thickness measurement locations on the battery. From the left to the right, a side and top view of the test configuration can be seen, followed by a schematic of the impactor geometry used. On the right-hand side, the positions at which the battery thickness were measured are marked with circles with different colours (four in the middle of the cell and one on each battery corner). This is followed by an image of the used test setup. (For interpretation of the references to colour in this figure legend, the reader is referred to the Web version of this article.)

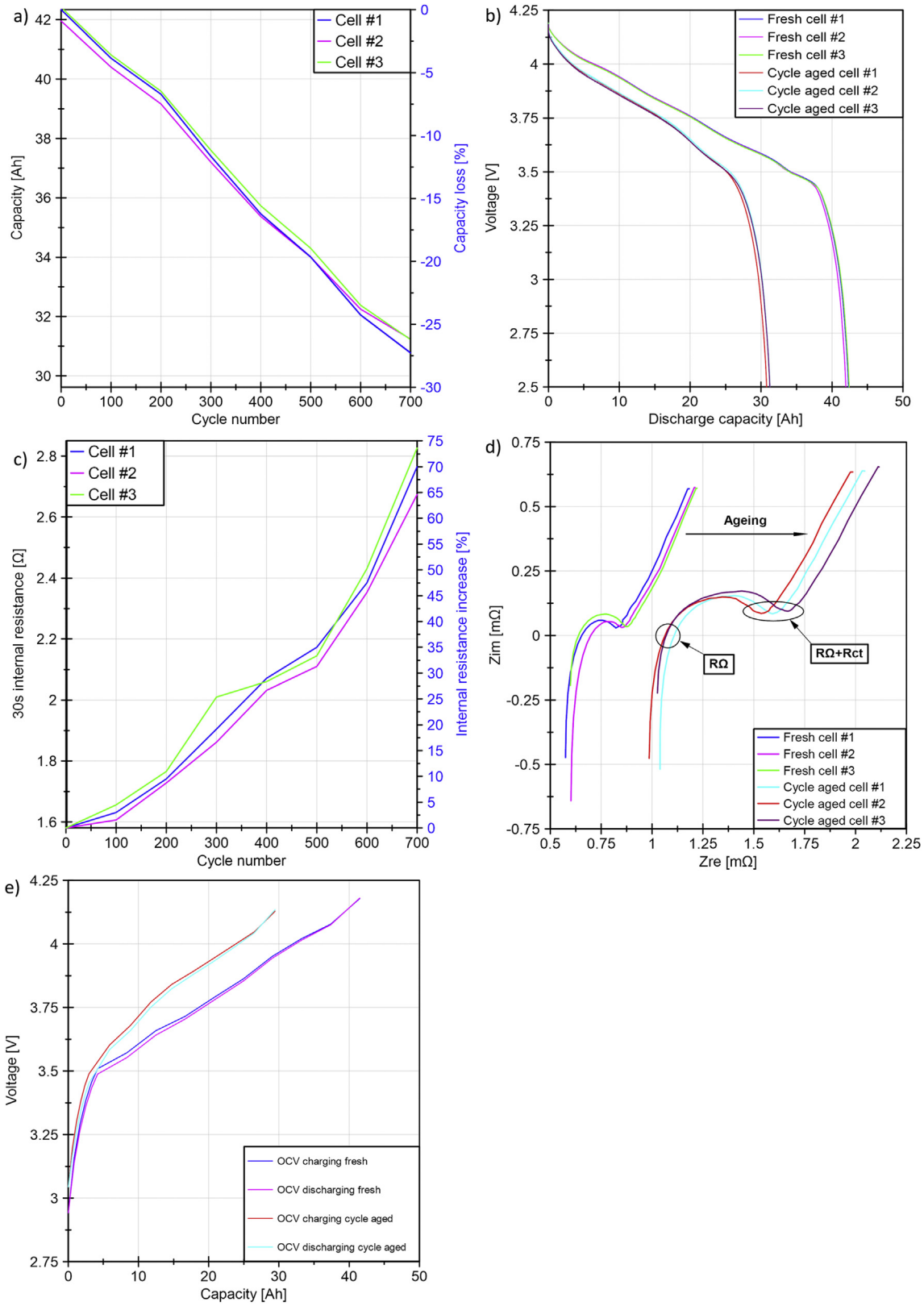

Fig. 2. Electrical characterisation data for fresh and aged cells. a) Capacity degradation of the investigated batteries with respect to cycle number. b) Discharge curves for fresh and aged batteries. C) Graph of the increase in internal resistance during ageing. d) Impedance spectra in form of a Nyquist plot, showing an increase in ohmic and charge transfer resistance for aged cells. e) Changed behaviour of the battery OCV curves after the end of the cycling procedure.

Table 1
Summary of the changes for different electrical parameters of the battery due to cycle ageing.

	C [Ah]	IR [mΩ]	R_Ω [mΩ]	R_{ct} [mΩ]
Fresh cell	42.23	1.62	0.66	0.21
Aged cell	31.08	2.74	1.08	0.59
Change [%]	**−26.51**	**+70.62**	**+62.73**	**+285.39**

An overall increase in the internal resistance of the batteries was measured in this study. As seen in Fig. 2c, with increasing cycle number the internal resistance also increases with a 10% average per 100 cycles during high-temperature cycling. In total, this results in an IR increase of 71%. Battery impedance also increased significantly after 700 cycles. In Fig. 2d, the EIS measurement results are visualised in the form of a Nyquist plot for both fresh and aged cells. A rise in the battery ohmic resistance is observed, which can be translated as a shift in the real axis of the zero-crossing point of the curve and the abscissa (R_Ω in Fig. 2d), indicating electrolyte and binder decomposition, current collector corrosion and oxidation of the conductive agent [8,15]. A change in the shape and size of the semicircle, displayed in Fig. 2d, can be interpreted as an increase in the charge transfer resistance (R_{ct}). This result correlates closely with the assumption that thicker SEI formed on the surface of the particles of the anode active material, which was also visualised during post-mortem analysis (Section 3.3). The formation of SEI resulted in a decrease in electrode porosity, which also translates into a higher R_{ct} [15]. The arithmetic mean values of the changed electrical parameters for aged cells as well the deviation of these values from the nominal values are presented in Table 1.

A small change in the slope of the linear region of the EIS spectrum is observed in Fig. 2d. This is a sign of a decreased diffusion of lithium ions, which is mainly caused by alterations in the active material of the negative electrode [15]. The OCV curve shape also changed with increased cycle life (Fig. 2e, red curve). The electrical behaviour of the investigated cells correlate with measurements made using different batteries with similar chemical compositions, which were aged under similar conditions [8,16].

3.2. Thickness measurements

Battery thickness was measured before and after the ageing procedure at several characteristic positions on the battery surface, as already mentioned in Section 2.4. The measurement results are displayed in Table 2.

An average thickness increase of about 0.55 mm was measured with the utilised measurement setup (6% of the overall cell thickness). This variation accounts for the irreversible swelling effect which lithium ion batteries experience after extensive charging and discharging. The continuous growth of the battery SEI on the anode layer surface, as well as gas generation and swelling in each charge-discharge cycle, are all factors that contribute to the final expansion of the cell. In Fig. 3, a box plot of the measured thicknesses of fresh and electrically aged batteries is provided, along with standard deviations from the mean arithmetic values.

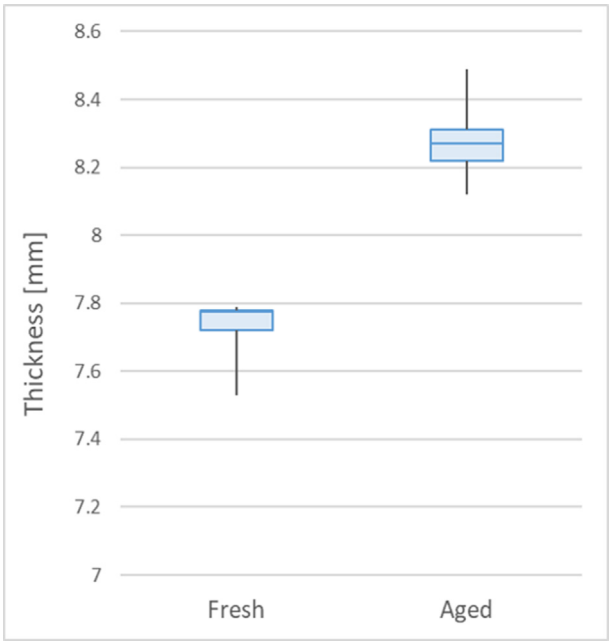

Fig. 3. Box plot of the measured thickness values with standard deviations from the shown arithmetic mean value.

3.3. Post-mortem analysis

In this section, not only the state of the battery electrodes after cell opening is discussed, but also the degradation mechanisms of each component, visualised with microscopic imaging techniques. The main degradation effects are identified that are responsible for the thickness increase in the investigated cell and for the changes in the electrical parameters. Results obtained in this section are used to explain differences in the electrical and mechanical behaviour of the battery before and after the cycling procedure.

3.3.1. Visual inspection of battery components

Two main differences were revealed during the visual inspection of the components of aged batteries after cell disassembly. The

Table 2
Measured thickness values for fresh and aged cells at eight characteristic battery locations (as seen on the right-hand side of Fig. 1).

Cell Status	Fresh			Aged		
Cell Position	Thickness Cell #1 [mm]	Thickness Cell #2 [mm]	Thickness Cell #3 [mm]	Thickness Cell #1 [mm]	Thickness Cell #2 [mm]	Thickness Cell #3 [mm]
Middle #1	7.78	7.79	7.78	8.38	8.39	8.24
Middle #2	7.78	7.78	7.78	8.34	8.22	8.33
Middle #3	7.78	7.77	7.77	8.31	8.35	8.2
Middle #4	7.79	7.79	7.79	8.28	8.29	8.26
Corner #1	7.65	7.57	7.67	8.33	8.28	8.22
Corner #2	7.75	7.78	7.73	8.32	8.25	8.31
Corner #3	7.59	7.67	7.53	8.33	8.29	8.37
Corner #4	7.78	7.75	7.77	8.25	8.23	8.24
Average Thickness [mm]	**7.74**	**7.74**	**7.73**	**8.31**	**8.28**	**8.27**

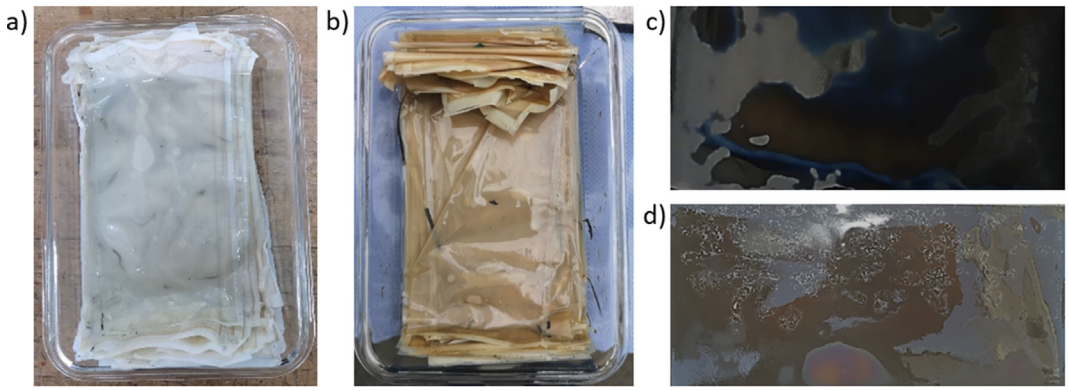

Fig. 4. Visual inspection of the battery components after cell disassembly. The two images on the left-hand side show a comparison of a) fresh and b) aged separators, whereby a distinct difference in colour is visible. The two images on the right-hand side show the differences between c) fresh and d) aged anode layers. On the aged anode, electrolyte salt deposits were clearly visible, indicating that part of the electrolyte was consumed during electrochemical ageing, leading to drying out of the battery. (For interpretation of the references to colour in this figure legend, the reader is referred to the Web version of this article.)

first was identified as a change in the colour of the separator as compared to a separator extracted from a fresh battery (Fig. 4a and b). A description of a general degradation mechanism that was found in the literature for cells with NMC chemistry is the dissolution of transition metals [16], which is believed to be one of the main causes of capacity degradation. Presence of manganese-containing compounds in the separator pores would thus explain the change in colour of the membrane. However, no Mn was detected by analysing the measured EDX spectrum on the separator (Section 3.3.2). An increased amount of carbon was measured, which would mean that graphite material in the form of small particles might have embedded in the porous separator after extended cycling. A small phosphorous (P) peak was also visible in the EDX spectrum, which suggests the presence of electrolyte decomposition products or lithium salts ($LiFP_6$) into the separator structure, which are most likely responsible for the brown coloration of the separator membrane.

The second difference was observed on the surface of every anode layer of the battery (Fig. 4d). Electrolyte salt deposits were also visible in the middle region of the cell, which is a sign of the consumption of the electrolyte solvent during the electrochemical cycling procedure.

3.3.2. Microscopy imaging

3.3.2.1. Anode. Most of the changes which occurred due to electrical ageing were observed at the battery anode. When investigating the surface of the anode active material, a thicker passivation layer (thicker SEI) was observed, which had formed on the graphite particles (Fig. 5a and b). The continuous growth of the SEI is in agreement with the consumption of active lithium and the high capacity loss. This growth also correlates with the measured increase in the internal resistance of all aged batteries and the increase in the size of the semicircle seen in the EIS spectra (Fig. 2d). During the investigation of the anode cross-section, the solid electrolyte interphase was visible as a thin shell around each graphite particle (Fig. 5j and k). At higher magnifications, besides the electrolyte salt remnants, which were also visible on the anode surface after cell disassembly (Fig. 4d), it was possible to identify small copper deposits on the surface of the anode active material (Fig. 5d, k). This was confirmed by the high Cu peaks of the EDX-spectrum (Appendix A. Fig. s3), recorded on a single small particle on the graphite surface. The copper particles were determined to be a product of corrosion of the copper current collector. The surface of the copper foil was strongly oxidised (Fig. 5e), leading to a transfer of Cu particles into the electrolyte and their redeposition onto the graphite surface. Copper oxidation was confirmed by Raman spectroscopy experiments, with results shown in Fig. 5g. During the cross-sectional investigations of the anode current collector, an oxide layer that was several hundred nanometres thick was measured on both sides of the copper layer (orange rectangles, Fig. 5f). Corrosion on contact between the current collector and the electrolyte can be excluded, because no traces of fluorine were found on the copper surface, as seen in the Raman spectrum. It is also possible to reject the hypothesis that copper dissolution occurred due to the fact that all batteries were opened while in a deep-discharged state (0 V), because no oxidation layer was observed on the surface of the fresh copper samples. The corrosion process on the copper current collector is more complex and may be related to the oxygen evolution that occurs at the cathode during the cycling procedure at 60 °C. The phenomenon of O2 release can originate from the bulk of oxygen-rich cathode particles and can be identified by the formation of defects and inter-/intragranular cracks [17]. These result from the mechanical stress that is induced by intercalation/deintercalation of lithium ions into/out of the lattice of the cathode. The oxygen that is produced reacts with the copper current collector, forming copper oxides and thus changing its surface structure and material properties. After it oxidizes, some of the Cu is solubilised from the surface of the current collector and redeposited on graphite particles. In Fig. 5i, the delamination of the anode active material from the Cu electrode can be seen, resulting from the altered adhesion properties of the current collector [18] and the loss of adhesion strength between the binder and the copper foil [19]. In terms of thickness, the active material of the aged anodes increased in size (Fig. 5i), as compared to the active material of samples extracted from fresh cells (Fig. 5h). This expansion contributes to the irreversible swelling of the batteries observed after electrical cycling. The increase in thickness (30 μm of the whole anode layer) results from the combined effect of a thicker SEI layer, which forms on the graphite particle surface, and the swelling of the binder.

3.3.2.2. Cathode. No additional layer was detected on the cathode surface, when the microscopic images of fresh with aged samples were compared (Fig. 6a and b). Surface imaging revealed cracks in the NMC particles of the blended active material of the cathode, which were more pronounced in the cross-sectional images of the positive electrode (Fig. 6c and d). The accumulation of microscopic defects on the NMC particle interface led to loss in mechanical strength and subsequent crack formation. This can be also accompanied by a reduction in the Young's modulus of NMC with

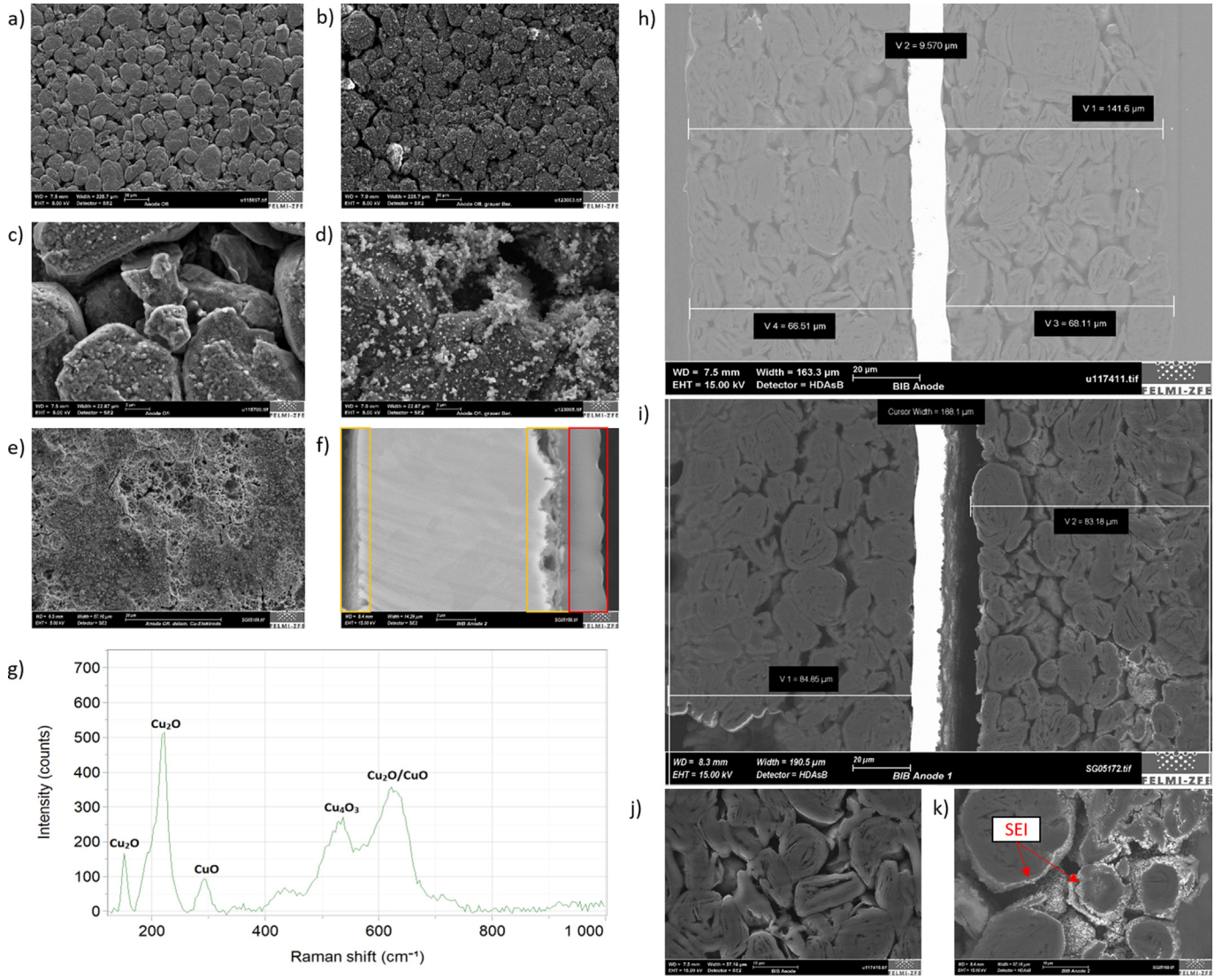

Fig. 5. Representation of the ageing mechanisms that occurred at the battery anode. a) Surface image of a fresh anode. b) Surface image of an aged anode, showing a thicker additional surface layer. C) Visualisation of the graphite particles of the fresh anode in more detail. d) magnified image of the aged anode active material, where not only the thicker SEI can be seen, but also small copper particles that were deposited on the anode surface. e) Visualisation of corrosion on the surface of the copper current collector of aged samples. f) Cross-sectional view of the aged copper current collector, showing a small additional oxide layer on both sides of the electrode (orange rectangle). The area marked with a red rectangle is an artefact due to the analysis methodology used. g) Raman spectrum of the aged copper layer, showing the formation of an oxide layer on its surface. h) Thickness measurement of the fresh anode. i) Thickness measurement of the aged anode layer, showing the thickness increase of the active material and the delamination of the graphite from the current collector. j) Fresh graphite layer in cross-section. k) Aged graphite layer in cross-section, showing a thin additional layer around the graphite particles (labelled as SEI). (For interpretation of the references to colour in this figure legend, the reader is referred to the Web version of this article.)

increasing cycle number, as stated in Refs. [20]. Visualizing cathode particle cracking also can be viewed as a confirmation of the hypothesis that oxygen is released from the cathode, as already mentioned above. After electrochemical ageing, no significant thickness changes were detected in the positive electrode (Fig. 6e and f). In addition, no delamination between aluminium and active material and no signs of current collector corrosion were observed.

3.3.2.3. Separator. SEM imaging revealed the presence of small particles that were deposited on the separator surface (Fig. 7b) as compared to fresh separator foils (Fig. 7a). EDX analysis was conducted on the polypropylene membrane (Fig. 7e) in order to identify the chemical composition of these reaction products. EDX spectra did not show any traces of copper as seen for the anode sample surface (Appendix A. Fig. s3). Transition metal peaks like Mn, Co or Ni were also not visible, however an increased amount of carbon was present, which would lead to the belief that a small amount of graphite material was embedded in the porous separator after extended cycling. The presence of phosphorous (P) would classify the visualised particles as lithium salt ($LiPF_6$) deposits. Due to its low energy of characteristic radiation, however, lithium cannot be detected with the standard EDX spectrometer and in order to confirm this statement a more advanced chemical composition determination method is needed. Nevertheless this would explain the change of colour of the separator foils, as already discussed in Section 3.3.1. As seen from the cross-section analysis of the aged separator samples, the bulk of the membrane was also contaminated with chemical reaction products (Fig. 7d, red circle). Intercalation of particles deep inside the pore structure of the separator resulted in a small increase in thickness of about 1 µm (Fig. 7g) compared to separators, taken out from fresh batteries (Fig. 7f). The increase in separator thickness would contribute to the

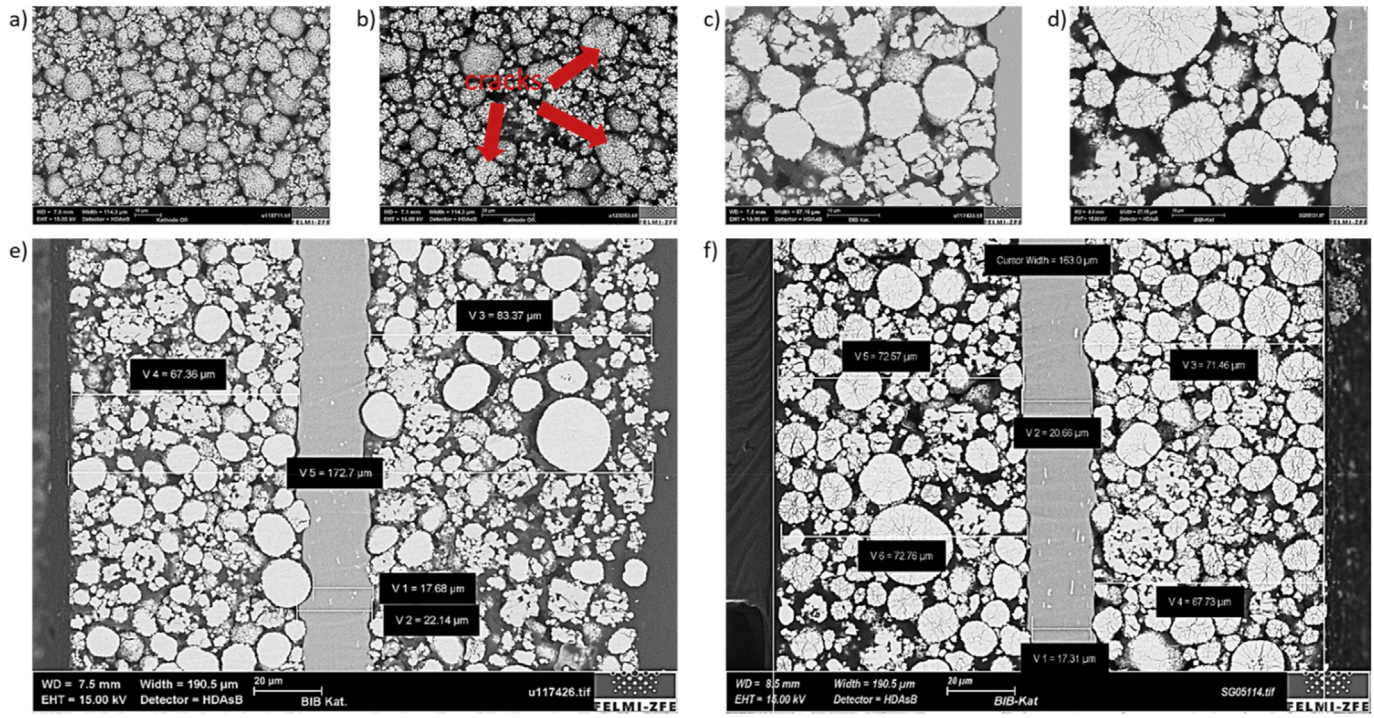

Fig. 6. Surface and cross-sectional analysis of the battery cathode. a) Surface image of the fresh cathode. b) Visualisation of the cathode structure of an aged sample, showing crack formation of the NMC particles. C) Cross-section of the active material of the cathode. d) Particle cracking as seen in cross section after the end of the cycling procedure. e) Measured thickness of the cathode active materials and current collector for fresh samples. f) Thicknesses measured for an aged positive electrode.

total thickness increase of the cell with about 40 µm.

3.4. Quasi-static mechanical tests

Quasi-static mechanical tests were performed under ambient temperature conditions to study the effect of battery degradation during high-temperature electrical cycling on the mechanical strength of the investigated pouch cell. A comparison between the indentation test results of fresh and electrically aged cells is shown in Fig. 8a. The mechanical resistance and battery deformation and voltage were measured during the test. An electrical short circuit for each cell is displayed as a voltage drop (Fig. 8a) after certain battery deformation occurred, which coincides with the global peak force, indicating the point of mechanical failure of all cells. All fresh cells started venting after electrical short circuit occurred at about a 1.5 mm impactor indentation depth. This event was followed by a rapid increase in internal temperature and, consequently, by a severe thermal runaway. The cell failure mechanism observed for aged batteries was different. At the point of mechanical failure, a 0.57 mm higher displacement was measured for the indenter, which accounted for a softer mechanical response of aged cells. While venting, the aged batteries produced noticeably less smoke before entering thermal runaway, and the TR process itself was less severe as seen in Appendix A. This event can be explained by the high capacity loss of the batteries determined at the end of the cycling procedure, as well as by the reduced amount of flammable electrolyte available. Cells were less reactive due to the reduced energy content.

Three main differences in the mechanical response of aged cells are shown in Fig. 8a. Electrically cycled cells displayed different behaviour at the start of the force/displacement characteristic (area marked with an orange rectangle) immediately after being placed in contact with the indenter up to an applied force of 100 kN. The force rise in this region is almost linear for fresh cells, whereas for aged cells the curve showed an exponential trend. This effect can be associated with the size evolution of the solid electrolyte interphase as the cycle number increases. In general the SEI layer can be described as a soft material with elastic-perfect plastic behaviour [21]. During battery ageing at high temperatures, the electrolyte is steadily consumed in electrochemical side reactions, contributing to the formation of a thicker SEI layer around the graphite particles (which are also visible in the cross-sectional images of the anode in Fig. 5k). During initial battery compression, the thicker solid electrolyte interphase contributes to the total behaviour of the cell, softening its overall mechanical response. This would explain the exponential force increase observed in the experimental test results for aged cells (red curves in Fig. 8). A visual representation of the effect, described above, can be seen in Fig. 8b. Graphite particles in the anode active material tend to differ in shape and size; however, they are tightly packed against one another. When a mechanical force acts on them, they are pressed against one another, leading first to an initial compression of the thicker SEI in the contact region between the particles and then to a subsequent particle compression. When the side reaction layer is fully compressed (100 kN mark in Fig. 8a, indicated as Δd in Fig. 8b), the measured force increases linearly as the battery is deformed. A slight change in the slope of the indentation curves of aged cells is also visible in Fig. 8a, which can be interpreted as a decrease in the overall stiffness of these batteries.

The second difference in the mechanical behaviour is indicated by the blue rectangle in Fig. 8a. The shift in displacement between the force/displacement curves for fresh and aged cells ($\Delta x = 0.57$ mm) can be easily explained by the results of the thickness measurements of aged batteries after 700 cycles (Table 2). Batteries cycled at high temperatures experienced an increase in thickness of about 0.55 mm, which correlates closely with the shift between green and red curves (Fig. 8a). Irreversible swelling is seen in this case due to the increase in the anode active

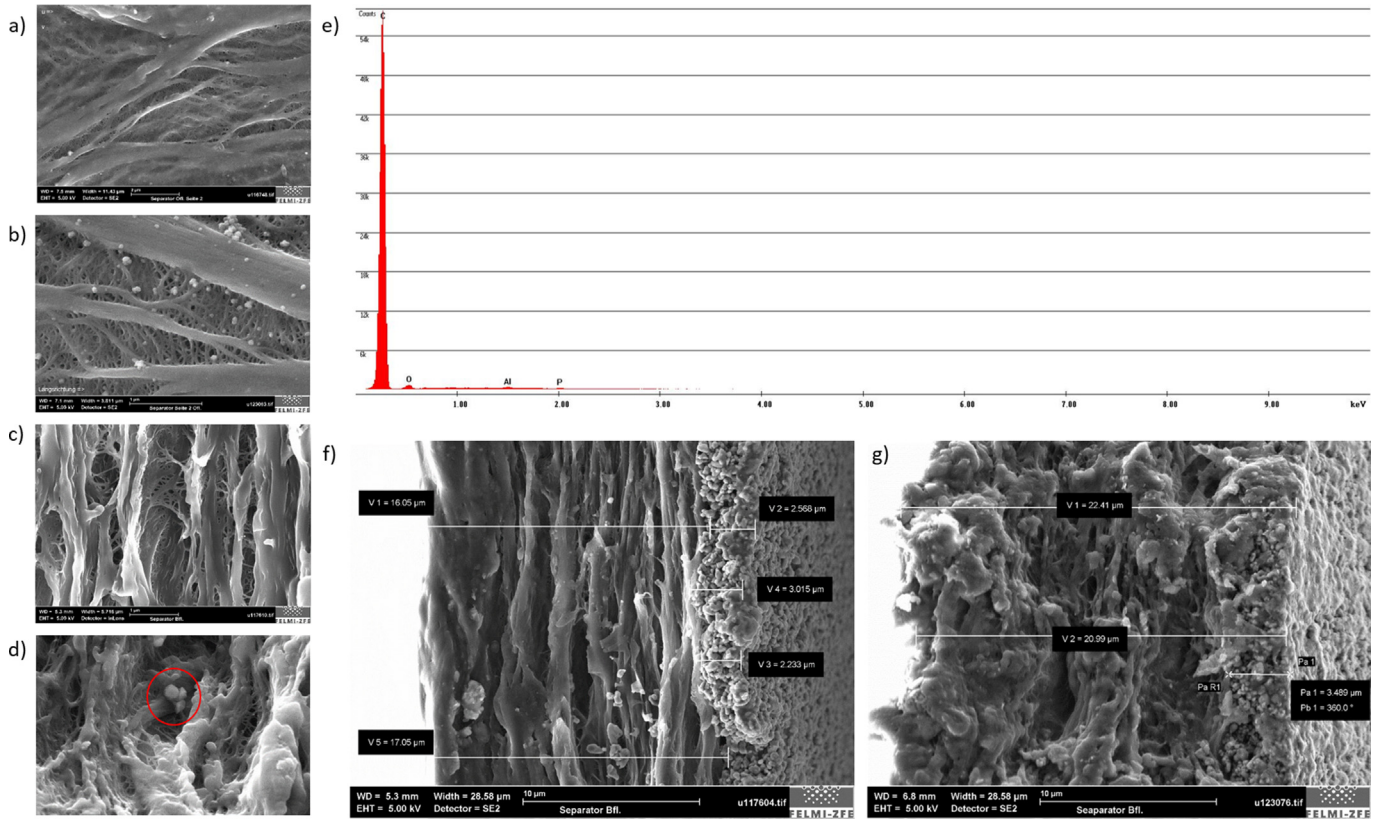

Fig. 7. Results of the post-mortem investigation conducted on fresh and aged separator samples. a) Surface image of the fiber structure of a fresh separator. b) Surface image of the aged separator, showing small particles intercalated in the separator pore structure. C) Fresh separator viewed in cross-section. d) Cross-sectional image of the aged separator, which shows that the small particles are also deposited in the bulk of the membrane. The fiber structure seems to be highly contaminated with deposits, which result from battery ageing. e) EDX spectrum conducted on the surface of an aged separator f) Measured thickness of fresh separator. g) Thickness determination for the aged separator, showing a minimal thickness increase of about 1 µm.

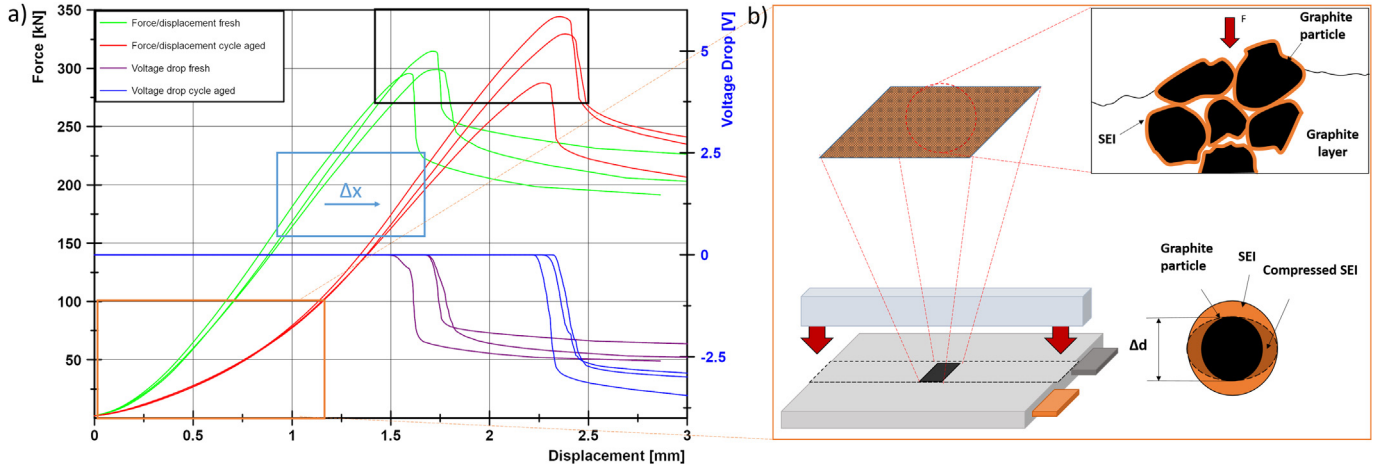

Fig. 8. Mechanical response of fresh and aged batteries under quasi-static indentation loads. a) Force displacement curves of fresh and aged batteries. Three main differences can be seen, as indicated by orange, blue and black rectangles. Aged batteries experienced an exponential force increase with respect to displacement up to the 100-kN indentation force and showed a shift in displacement of 0.57 mm and an increased peak force at the point of cell failure. Shown is also the voltage drop at a specific displacement for fresh and aged batteries, which coincides with the drop in force level. b) The model that was used to explain the mechanical response of aged batteries during the initial compression stage up to the point of a 100 kN applied force. The initial compression of the more elastic SEI layer results in an observed exponential increase in the force/displacement curve for aged batteries. (For interpretation of the references to colour in this figure legend, the reader is referred to the Web version of this article.)

material size (Fig. 5i), as well as to the intercalation of particles in the separator fibre structure (Fig. 7d), thus slightly increasing the separator thickness.

Regarding the maximum force measured at the point of cell failure, the aged batteries could withstand higher indentation forces under the test conditions (black rectangle in Fig. 8). An average peak force difference of about 30 kN was measured during mechanical testing. An explanation to this effect can be found by

Table 3
EUCAR hazard level classification sheet as seen in Ref. [30].

EUCAR hazard level classification sheet	
0 No effect	No effect, no loss of functionality
1 Passive protection activated	No leakage, no venting, no fire or flame, no rupture, no explosion, no exothermic reactions or thermal runaway, cell reversibly damaged, repair of protection device needed
2 Defect Damage	No leakage, no venting, no fire or flame, no rupture, no explosion, no exothermic reactions or thermal runaway, cell irreversibly damaged, repair needed
3 Leakage >50%	No Fire or flame, no rupture, no explosion, weight loss $\leq$50% of the electrolyte weight electrolyte = solvent + salt
4 Venting >50%	No fire or flame, no rupture, no explosion, weight loss $\geq$50% of the electrolyte weight
5 Fire or Flame	No rupture, no explosion, i.e. no flying parts
6 Rupture	No explosion, but flying parts, ejection of parts of active mass
7 Explosion	Explosion, i.e. disintegration of the cell

analysing the battery degradation mechanisms in more detail. As the cycle number increases, batteries tend to lose capacity due to side reactions of lithium with the electrolyte at the anode/electrolyte interface [22,23]. This not only results in a loss of lithium inventory [14], but in a decrease in the electrolyte content inside the cell [6]. The faster voltage decrease, visible at the beginning of the discharge curves of aged batteries (Fig. 2b), is an indication for the consumption of electrolyte [24]. The effect of the cell drying out was also confirmed after the cells were opened (Section 3.3.1). Dried-out regions on the battery anode were discovered, where electrolyte salt deposits were visible on the surface. Under a mechanical load, cells with less electrolyte content experience an increase in peak force at the point of mechanical failure [25]. This effect originates from structural changes that take place in the active material of the electrodes during battery cycling or, more precisely, in the binding material. Due to changes in their crystalline structure, the elasticity of PVDF (polyvinylidenefluoride) binders reduces by about 30% after electrochemical ageing of cells to 80% of their original state of health (SOH) [26], resulting in an increase in material hardness. A second reason for the increase in peak force is the change that occurs in the mechanical behaviour of polypropylene separators in wet and dry state. When soaked in electrolyte, the Young's modulus of polypropylene (PP) separators decreases [27–29]. As the amount of electrolyte decreases in aged cells, the mechanical response of the separator hardens and, thus, contributes to the increased force levels observed at cell failure.

3.5. Safety assessment

In order to make an accurate safety assessment, several factors need to be taken into consideration. During the mechanical tests for aged cells, a less severe thermal runaway process was detected (Appendix A. Fig. s1) as compared to that of fresh batteries. After electrical failure occurred, which was coincident with the mechanical failure, aged cells started venting, whereby only two out of three batteries caught on fire. The intensity of the flames for aged cells was noticeably lower, presumably due to the high capacity loss determined after battery cycling and to the resulting reduced electrolyte content. These cells could still be classified as hazard level 5, referring to the EUCAR hazard level classification sheet [30] (Table 3), however a trend pointing towards hazard level 4 can be seen due to the less violent behaviour of aged batteries after failure.

The investigated electrically aged batteries can be considered less hazardous than fresh cells, taking also into consideration the softer mechanical response observed during mechanical indentation tests (Section 3.4) and the higher peak forces observed at the onset of mechanical failure.

3.6. Limitations and prospects

The result and findings reported in this work may differ when testing batteries cycled under different conditions, different types of batteries, or cells with different chemistries. The mechanical behaviour of batteries may also change if it is subjected to different load cases or when other indenter geometries are used. To better understand the mechanical response of aged cells, more tests should be conducted in future studies to more thoroughly examine the influence of differences among cells due to cell manufacturing and to draw more statistically valid conclusions.

4. Conclusion

In the presented paper, the electrical performance of cycle aged lithium-ion batteries and their behaviour under a quasi-static indentation load were reported. A detailed post-mortem analysis revealed the main degradation effects responsible for the occurred changes in the electrical and mechanical response of electrically aged cells.

The investigated lithium-ion pouch cells included in this study displayed a reduction in useable cell capacity and an increase in internal resistance and impedance after being cycled at elevated temperatures. These changes were ascribed to the loss of lithium inventory, where active lithium is consumed in electrochemical side reactions to form a thicker SEI on the anode surface. The growth of an additional layer on the graphite particles, the electrolyte consumption, copper corrosion and the cracking of particles of the active material of the cathode were identified as the main degradation effects resulting from battery electrical ageing.

Under quasi-static indentation loads, the current electrically aged batteries have shown a softer mechanical response. They experienced an exponential force increase up to 30% of the maximum measured force, which was associated with an initial compression of the thicker SEI, visible on the anode active material surface. A shift in the displacement values of about 26% was observed when comparing the results of fresh and aged batteries. This was a consequence of the irreversible swelling of the battery due to cycle ageing (6% thickness increase), reasons for which are the increased thicknesses of the anode active material and of the battery separator. A slight reduction in the stiffness of aged cells was observed, identified as a change in the slope of the force-displacement curves. Aged batteries were able to withstand higher force levels at the onset of cell failure, which was ascribed to the electrolyte consumption, leading to changes in the mechanical properties of the battery separator and of the active materials of the electrodes.

The results of this work allow the conclusion to be drawn that cycle ageing at elevated temperatures of the investigated battery results in less hazardous cells, behaving safer under quasi-static mechanical crush loads with a flat impactor. This conclusion is drawn based on the mechanical response of the batteries and on the severity of the thermal runaway process after cell failure. This work can be classified as a first attempt to explain the interaction

between electrical ageing conditions, degradation mechanisms and mechanical behaviour of lithium-ion batteries. In order to draw more general conclusions about the hazard level of aged cells under mechanical loads, sufficient experimental data are needed for cells with different chemical compositions and that have been cycle aged under different aging conditions. The collection and evaluation of such data is set as a goal in future investigations.

CRediT authorship contribution statement

Georgi Kovachev: Conceptualization, Methodology, Investigation, Writing - original draft. **Christian Ellersdorfer:** Project administration. **Gregor Gstrein:** Conceptualization, Writing - review & editing. **Ilie Hanzu:** Writing - review & editing. **H. Martin R. Wilkening:** Writing - review & editing. **Tobias Werling:** Writing - review & editing. **Florian Schauwecker:** Writing - review & editing. **Wolfgang Sinz:** Supervision, Writing - review & editing.

Declaration of competing interest

The authors declare that they have no known competing financial interests or personal relationships that could have appeared to influence the work reported in this paper.

Acknowledgements

This work was conducted as part of the research project SafeBattery. The COMET project SafeBattery is funded within the framework of COMET — Competence Centers for Excellent Technologies by BMVIT, BMDW and the Province of Styria as well as SFG (Grant No. 863073). The COMET Program is managed by FFG. The authors thank the consortium members of SafeBattery project for supporting this work.

Appendix B. Supplementary data

Supplementary data to this article can be found online at https://doi.org/10.1016/j.etran.2020.100087.

References

[1] Lu L, Han X, Li J, Hua J, Ouyang M. J Power Sources 2013;226:272–88. https://doi.org/10.1016/j.jpowsour.2012.10.060.
[2] Rizoug N, Sadoun R, Mesbahi T, Bartholumeus P, LeMoigne P. IET Electr Syst Transp 2017;7:14–22. https://doi.org/10.1049/iet-est.2016.0012.
[3] Daberechi DA, Opara F, Chukwuchekwa N. Review of comparative battery energy storage systems (bess) for energy storage applications in tropical enviroments. IEEE Nigercon 2017:1000–5.
[4] Shim J. J Power Sources 2002;112:222–30. https://doi.org/10.1016/S0378-7753(02)00363-4.
[5] Ma S, Jiang M, Tao P, Song C, Wu J, Wang J, Deng T, Shang W. Prog Nat Sci: Materials International 2018;28:653–66. https://doi.org/10.1016/j.pnsc.2018.11.002.
[6] Han X, Lu L, Zheng Y, Feng X, Li Z, Li J, Ouyang M. eTransportation 2019;1:100005. https://doi.org/10.1016/j.etran.2019.100005.
[7] Mu L, Lin R, Xu R, Han L, Xia S, Sokaras D, Steiner JD, Weng T-C, Nordlund D, Doeff MM, Liu Y, Zhao K, Xin HL, Lin F. Nano Lett 2018;18:3241–9. https://doi.org/10.1021/acs.nanolett.8b01036.
[8] Stiaszny B, Ziegler JC, Krauß EE, Schmidt JP, Ivers-Tiffée E. J Power Sources 2014;251:439–50. https://doi.org/10.1016/j.jpowsour.2013.11.080.
[9] Ren D, Lu L, Ouyang M, Feng X, Li J, Han X. Energy Procedia 2017;105:2698–704. https://doi.org/10.1016/j.egypro.2017.03.919.
[10] Wu Z, Cao L, Hartig J, Santhanagopalan S. ECS Trans 2017;77:199–208. https://doi.org/10.1149/07711.0199ecst.
[11] Zhang X, Zhu J, Sahraei E. RSC Adv 2017;7:56099–107. https://doi.org/10.1039/c7ra11585g.
[12] Kovachev Schröttner, Gstrein Aiello, Hanzu Wilkening, Foitzik Wellm, Sinz Ellersdorfer. Batteries 2019;5:67. https://doi.org/10.3390/batteries5040067.
[13] Oetjen G-W, Haseley P. In: Freeze-drying, 2nd completely rev. and extended. Weinheim, Cambridge: Wiley-VCH; 2004. Georg-Wilhem Oetjen, Peter Haseley.
[14] Birkl CR, Roberts MR, McTurk E, Bruce PG, Howey DA. J Power Sources 2017;341:373–86. https://doi.org/10.1016/j.jpowsour.2016.12.011.
[15] Gao Q, Dai H, Wei X, Jiang B. https://doi.org/10.4271/2019-01-0596; 2019.
[16] Buchberger I, Seidlmayer S, Pokharel A, Piana M, Hattendorff J, Kudejova P, Gilles R, Gasteiger HA. J Electrochem Soc 2015;162:A2737–46. https://doi.org/10.1149/2.0721514jes.
[17] Sharifi-Asl S, Lu J, Amine K, Shahbazian-Yassar R. Adv. Energy Mater. 2019;9:1900551. https://doi.org/10.1002/aenm.201900551.
[18] Dai C, Wang Z, Liu K, Zhu X, Liao X, Chen X, Pan Y. Eng Fail Anal 2019;101:193–205. https://doi.org/10.1016/j.engfailanal.2019.03.015.
[19] Chen J, Liu J, Qi Y, Sun T, Li X. J Electrochem Soc 2013;160:A1502–9. https://doi.org/10.1149/2.088309jes.
[20] Xu R, Sun H, de Vasconcelos LS, Zhao K. J Electrochem Soc 2017;164:A3333–41. https://doi.org/10.1149/2.1751713jes.
[21] Yoon I, Jurng S, Abraham DP, Lucht BL, Guduru PR. Energy Storage Materials 2020;25:296–304. https://doi.org/10.1016/j.ensm.2019.10.009.
[22] Vetter J, Novák P, Wagner MR, Veit C, Möller K-C, Besenhard JO, Winter M, Wohlfahrt-Mehrens M, Vogler C, Hammouche A. J Power Sources 2005;147:269–81. https://doi.org/10.1016/j.jpowsour.2005.01.006.
[23] Kabir MM, Demirocak DE. Int J Energy Res 2017;41:1963–86. https://doi.org/10.1002/er.3762.
[24] Günter FJ, Burgstaller C, Konwitschny F, Reinhart G. J Electrochem Soc 2019;166:A1709–14. https://doi.org/10.1149/2.0121910jes.
[25] Kisters T, Sahraei E, Wierzbicki T. Int J Impact Eng 2017. https://doi.org/10.1016/j.ijimpeng.2017.04.025.
[26] Wendt C, Niehoff P, Winter M, Schappacher FM. J Power Sources 2018;391:80–5. https://doi.org/10.1016/j.jpowsour.2018.03.064.
[27] Yan S, Xiao X, Huang X, Li X, Qi Y. Polymer 2014;55:6282–92. https://doi.org/10.1016/j.polymer.2014.09.067.
[28] Gor GY, Cannarella J, Leng CZ, Vishnyakov A, Arnold CB. J Power Sources 2015;294:167–72. https://doi.org/10.1016/j.jpowsour.2015.06.028.
[29] Sheidaei A, Xiao X, Huang X, Hitt J. J Power Sources 2011;196:8728–34. https://doi.org/10.1016/j.jpowsour.2011.06.026.
[30] Doughty DH, Crafts CC. https://doi.org/10.2172/889934; 2005.

Glossary

NMC: $LiNiMnCoO_2$
LMO: $LiMn_2O_4$
BMS: battery management system
IR: internal resistance
LLI: loss of lithium inventory
LAM: loss of active material
LIB: lithium ion batteries
SOC: state of charge
SEM: scanning electron microscopy
EV: electric vehicle
SEI: solid electrolyte interphase
RPT: reference performance test
OCV: open circuit voltage
EIS: electrochemical impedance spectroscopy
IR: internal resistance
CCCV: constant current constant voltage
CC: constant current
FESEM: field scanning electron microscope
EDXS: energy dispersive x-ray spectroscopy
BIB: broad ion beam
R_Ω*:* ohmic resistance
R_{ct}*:* charge transfer resistance
C_{dl}*:* double layer capacitance
Cu: copper
SOH: state of health
PVDF: polyvinylidene fluoride